SAN096-2647C

SAND--96-2647C

CONF-9609303--1

FUNDAMENTALS OF SOL-GEL FILM DEPOSITION

PI: C. J. Brinker

Research Team:
Mark T. Anderson (SNL)
Rahul Ganguli (UNM graduate student)
Yungfeng Lu (UNM graduate student)
Mengcheng Lu (UNM graduate student)
Teresa Bohuszewicz (SNL)

Funding: $~50K 4/01/96 to 4/01/97

Goal: A fundamental understanding of sol-gel thin film deposition is necessary to develop inorganic thin films for applications as membranes, low dielectric constant interlayers, and protective coatings. The expanded goal of this project is to examine sol-gel thin film deposition from a fundamental basis that addresses both defect formation (cracks, delamination, etc.) and microstructure development.

Accomplishments: In the preceding six months of this project, we began to explore the role of surfactant additions on microstructural development of sol-gel films deposited by dip-coating with the primary goal of elucidating processing schemes to form closed porosity, low dielectric constant coatings and thick crack-free layers. Highlights of this initial study are:

1) Surfactant additions to acid-catalyzed silica sols were shown by XRD, TEM, and SAW-sorption studies to result in the development of porous, ordered *meso*structures with pores sizes ranging from 10 - 50Å.
2) Processing parameters such as surfactant concentration, water concentration, sol aging, and processing ambient were all found to systematically vary the thin film microstructure.
3) Films containing over 50% porosity and exhibiting open or closed porosity were prepared.
4) Surfactant additions enable the formation of thick films without cracking.
5) Pre-treatment of substrate surfaces with hydrophobic or hydrophilic SAMs directs resulting microstructural development.

1. Background - Surfactant Templating of Mesoporous Silica

Surfactants are bifunctional molecules that contain a solvent-loving (lyophilic) head group and a solvent-hating (lyophobic) tail (i.e. they are amphiphiles). As a result of their amphiphilic nature, surfactants can associate into supramolecular arrays. For example, cetyltrimethylammonium bromide ($CH_3(CH_2)_{15}N(CH_3)_3^+Br^-$ or $C_{16}TMABr$) in water will form spherical micelles that contain ~90 molecules. In the micelle, the hydrophilic head groups form the outer surface and the hydrophobic tails point toward the center. This arrangement minimizes the unfavorable interaction of the tails with water, but introduces a competing unfavorable interaction, the repulsion of the charged head groups. The balance between these competing factors determines the relative stability of the micelles.

The extent of micellization, the shape of the micelles, and the aggregation of micelles into liquid crystals depends on the surfactant concentration. A schematic phase diagram for a cationic surfactant in water is shown in **Figure 1.** At very low concentration, c, the surfactant is present as free molecules dissolved in solution and adsorbed at interfaces.

This work was supported by the United States Department of Energy under Contract DE-AC04-94AL 85000.
Sandia is a multiprogram laboratory operated by Sandia Corporation, a Lockheed Martin Company, for the United States Department of Energy.

DISCLAIMER

At slightly higher concentrations, called the critical micelle concentration (CMC1), the individual surfactant molecules form small, spherical aggregates (micelles). At higher concentrations (CMC2), where the amount of solvent available between the micelles decreases, spherical micelles can coalesce to form elongated cylindrical micelles.

At slightly higher concentrations, liquid crystalline (LC) phases form. Initially, rod-like micelles aggregate to form hexagonal close-packed LC arrays. As the concentration increases, cubic bicontinuous LC phases form followed by LC lamellar phases. At very high concentrations, in some systems, inverse phases can exist. Here water is solubilized at the interior of the micelle and the head groups point inwards.

Synthesis of Surfactant/Inorganic Mesophases

Surfactants with a wide variety of sizes, shapes, functionalities, and charges have recently been used to form *bulk* (primarily silica) mesophases. The surfactants are classified based on their head group chemistry and charge: Anionic – the hydrophilic group carries a negative charge; examples include sulfates ($C_nH_{2n+1}OSO_3$ (n = 12, 14, 16, 18), sulfonates ($C_{16}H_{33}SO_3H$ and $C_{12}H_{25}C_6H_4SO_3Na$), phosphates ($C_{12}H_{25}OPO_3H_2$, $C_{14}H_{29}OPO_3K$), and carboxylic acids ($C_{17}H_{35}COOH$ and $C_{14}H_{29}COOH$). Cationic – the hydrophilic group carries a positive charge; examples include alkylammonium salts, such as, $(C_nH_{2n+1}(CH_3)_3NX$, n = 6 (non mesophase), 8, 9, 10, 12, 14, 16, 18, 20, 22; X = OH/Cl, OH, Cl, Br, HSO_4 and $C_nH_{2n+1}(C_2H_5)_3N$, n = 12, 14, 16, 18), gemini surfactants $[C_mH_{2m+1}(CH_3)_2N\text{-}C_sH_{2s}\text{-}N(CH_3)_2C_mH_{2m+1}]Br_2$, m = 16, s = 2-12) cetylethylpiperidinium salts ($C_{16}H_{33}N(C_2H_5)(C_5H_{10})^+$); and bichain salts (dialkyldimethylammonium). Nonionic - the hydrophilic group is not charged; examples include primary amines ($C_nH_{2n+1}NH_2$) and polyoxyethylene oxides, octaethylene glycol monodecyl ether ($C_{12}EO_8$) and octaethylene glycol monohexadecyl ether ($C_{16}EO_8$). A fourth class, amphoteric (and zwitterionic), exists, but no reports of their use are known.

To synthesize periodic mesoporous silica, four reagents are generally required: water, a surfactant, a silica source, and a catalyst. Pure silica mesophases, exhibit three structure types: hexagonal (H; or MCM-41), a 1-d system of hexagonally arrayed cylindrical pores; cubic (C), a 3-d, bicontinuous system of pores (*Ia3d* and *Pm3n*); lamellar (L), a 2-d system of metal oxide sheets interleaved by surfactant bilayers (probably many closely related structures of this type). In the latter, the structure collapses when the template is removed, so it is of less interest. In each type there is a periodic arrangement of pores (or layers), but the inorganic walls (or sheets) are amorphous. In addition a variety of less well ordered phases have been observed. These materials generally exhibit one low angle diffraction peak, have narrow pore size distributions and high surface areas.

Extension to Thin Film Formation

Mesoporous silicas typically form as precipitates that are unsuitable for film formation. Our idea is to start with a homogeneous sol prepared with a surfactant concentration below CMC1 (see **Figure 1**) and exploit solvent evaporation during thin film deposition to concentrate the surfactant in the depositing film, causing the progressive development of mesoporous phases in the depositing film (see **Figure 2**). Solidification of the film by gelation near the drying line should "freeze-in" a particular mesoscopic structure. By varying the initial surfactant concentration we should be able to develop a family of mesoporous silica films ranging in structure from entrapped spherical micelles to hexagonal, cubic, and lamellar liquid crystals. Pyrolysis (or solvent extraction) of the surfactants then is used to create the corresponding mesoporous film (assuming that the surfactant templates can be removed without collapse of the silica framework). For the case of occluded spherical micelles, it is expected that pyrolysis and removal of organics could occur via diffusion through the microporous silica matrix at intermediate temperatures followed by sintering of the matrix at higher temperatures to create closed porosity films.

Additional roles of surfactants in thin film formation

It is well established that surfactants organize at liquid-vapor interfaces where they can significantly depress the equilibrium surface tension γ_{LV}. This reduces the maximum capillary stress P_c developed during drying:

$$P_C = -\gamma_{LV}/r_m = -2\gamma_{LV}\cos(\theta)/r_p, \quad (1)$$

where θ is the wetting angle and r_p is the pore size. This results in turn in an increased critical cracking thickness h_C (the maximum thickness below which cracking is observed not to occur):

$$h_C = (K_{IC}/P_c\Omega)^2, \quad (2)$$

where K_{IC} is the critical stress intensity or "fracture toughness" and Ω is a function that depends on the ratio of the elastic modulus of the film and substrate (for gel films $\Omega \cong 1$). Thus in addition to influencing film microstructure, surfactant additions are anticipated to reduce the drying stress and tendency for cracking.

2. Synthesis Procedures

122 ml TEOS, 122ml absolute ethanol, 9.74 ml deionized water, and 0.4 ml 0.07N hydrochloric acid were mixed at 60 °C for 90 minutes forming a stock solution. To 15 ml of the stock solution varying concentrations of de-ionized water, ranging from 2 - 6.8 weight %, and 1.8 ml of 0.07N hydrochloric acid was added. This mixture was stirred for 15 minutes and diluted with twice the volume of absolute ethanol. To this sol, CTAB (cetyltrimethylammonium bromide) was added in concentrations ranging from 1.0 to 5.0 weight %.

Films were deposited on <100> silicon wafers or crystalline quartz SAW substrates by dip-coating at rates ranging from 20 - 50 cm/min. Films were characterized by XRD, ellipsometry, TEM, and SAW-based N_2 sorption before and after pyrolysis in air at 400°C (1°C/min heating and cooling rates and 4 h hold time). A limited number of films were deposited on self-assembled monolayers (SAMs) prepared on gold substrates with either hydrophilic (carboxylate) or hydrophobic (methyl) surfaces, using $HS(CH_2)_{16}COOH$ and $HS(CH_2)_3CH_3$, respectively.

3. Results and Discussion

Effect of surfactant concentration

The effect of surfactant concentration was evaluated by XRD experiments performed before and after calcination (see **Figures 3(a) and (b)**). Figure 3(a) shows XRD results for uncalcined films. With increasing surfactant concentration there is a shift from broad features at low angle to progressively sharper features at higher angles (the exception being the 3.0% sample). The 2.0 and 2.5 % samples showed low angle peaks (d = 40.58 and 40.87Å, respectively) attributable to <100> peaks of the hexagonal LC phase. The sharper peaks observed for the 4.0, 4.5, and 5.0% samples (d = 34.7, 34.3, and 34.5Å, respectively) are consistent with lamellar phases. Both the 2.5 and 3.5% samples exhibited two peaks suggesting the formation of composite structures comprising two hexagonal phases (2.5% sample) or a mixture of hexagonal and lamellar phases (3.5% sample).

Figure 3(b) shows the corresponding XRD patterns after calcination at 400°C. In general there is a shift of all the peak features to higher angles consistent with consolidation of the film structures. All the peaks attributable to lamellar phases are observed to broaden significantly, compared to those associated with hexagonal phases. This suggests that the lamellar phases collapse to varying degrees upon surfactant pyrolysis, whereas the hexagonal phases experience a uniform densification (due to continued condensation of the silica framework), preserving the periodicity and uniformity of the pore size. Surfactant concentrations below 2.0% result in weakly ordered or completely disordered films. It is interesting to note that the 2.5% sample maintains its composite structure, whereas the 3.5% sample exhibits only one peak corresponding to the hexagonal phase.

The effect of water concentration was studied by preparing a series of sols containing 2.5 weight % surfactant and water concentrations ranging from 2 - 20 weight %. **Figures 4(a) and (b)** show the XRD results for this series of films before and after calcination, respectively. We see that, for the uncalcined films, increasing water concentrations cause a dramatic sharpening then broadening of the peak shape along with a shift of the peak position to lower angles. The prominent peaks observed for the 5.9 and 6.8% water samples (d = 39.5Å) are attributable to the <100> reflections of the hexagonal phase. The corresponding <200> reflections (d = 19.5Å) are also visible. At water concentration of 10% and above, broad features are observed at low angles. After calcination, the peaks are generally shifted to higher angles consistent with shrinkage of the silica framework. However there again appears a progressive sharpening then broadening of the peak shape with increasing water concentration. The 6.8% water sample exhibits peaks attributable to <100> (d = 32.5Å) and <200> (d = 16.5Å) reflections of the hexagonal phase.

Structures of calcined films prepared with 2.5 wt% surfactant and varying water concentrations were further evaluated by TEM and ellipsometry. TEM samples were prepared as thin flakes or as thin sections observed in plan or cross-sectional orientations. All samples prepared with water concentrations ranging from 5.9 to 50 % show uniformly sized pores. The pore size increases with water concentration from ~25Å for the 5.9% water sample to ~50Å for the 50% water sample. Some ordering of the porosity is observed in the 5.9% water sample, while the 6.8% water sample shows periodically arranged pore channels in plan view. Cross-sectional TEM of the 6.8% water sample (see **Figure 5**) shows highly ordered regions at both the substrate-film and film-vapor interfaces indicative of pore channels oriented parallel to these interfaces. The interior of the film is poorly ordered but exhibits a uniform texture consistent with a uniform pore size.

Ellipsometry was used to determine the thickness and refractive index of selected films. The refractive index values were used in turn to calculate the film porosity using the Lorentz-Lorenz relationship and assuming a refractive index of 1.46 for the silica framework. The 5.9 and 6.8% water samples were both 370 nm thick. The refractive indices were measured to be 1.21 and 1.19 corresponding to 52 and 56% porosity, respectively. The 10% water sample was 160 nm thick with a refractive index of 1.40, corresponding to about 10% porosity.

Our idea is that the film mesostructure develops progressively and that the final film structure is "frozen-in" at the drying line (see Figure 2). Therefore it might be anticipated that the uniformity and degree of ordering of the pore structure would be sensitive to the process time scale, which is governed by the evaporation rate. To address this issue, we prepared sols containing 5 weight % surfactant and deposited films under conditions in which the ambient relative humidity (RH) was varied from about 0 - 90%. XRD patterns of the samples prepared at 0 - 50% RH are essentially featureless. The film deposited at RH = 70% shows a weak shoulder at d= 20.6Å. The film deposited at 80% RH shows a broad peak at about d = 17.4Å, and the film deposited at 90% RH shows a strong sharp peak at d = 18Å and a relatively weaker, broader peak at d = 37Å. TEM reveals that films prepared over the range 0 - 80% RH are disordered, whereas the film prepared at

90% RH is a well-ordered layered structure with a layer spacing of about 18Å. These results suggest that by suppressing the evaporation rate of water, and thereby protracting the film deposition time scale, greater ordering of the silica-surfactant assembly is achieved.

The accessible porosity of the deposited films has been measured directly for several thin film samples using surface acoustic wave (SAW)-based N_2 sorption. **Figure 7** shows SAW N_2 adsorption-desorption isotherms for two samples shown to contain ordered mesoporosity by XRD and refractive index measurements. Despite similar pore sizes, one sample exhibits open porosity and the other, apparently closed porosity. For the sample exhibiting open porosity the isotherm shows absolutely no hysteresis consistent with a system of uniformly sized mesopores. From the volume adsorbed at high relative pressure, we calculate a porosity of about 55% consistent with the ellipsometry results. We suspect that the sample showing no N_2 accessibility has a skin consisting of a collapsed lamellar structure or perhaps an aligned hexagonal structure characterized by a highly tortuous diffusion pathway. Preliminary TEM cross-sectional analyses appear to support this hypothesis (see Fig. 5).

In an effort to control pore orientation at the film-substrate interface, films were deposited on hydrophobic or hydrophilic self assembled monolayers under identical processing conditions. XRD analysis of the corresponding films shows that the nature of the SAM surface can completely control the pore size and periodicity.

Summary and Conclusions

Results to date appear to confirm our concept of surfactant-templating of thin film mesostructures as depicted in Figure 2. We have shown that the final film pore structure depends on the starting surfactant and water concentrations along with the process time scale (governed by the evaporation rate). With increasing initial surfactant concentration we vary the pore structure systematically from disordered to hexagonal to lamellar. We have shown examples of composite structures (hexagonal + lamellar) that might represent transitional structures or graded structures kinetically "frozen-in" by gelation. Surfactant ordering at the substrate-film and film-vapor interfaces serves to orient the porosity of the adjoining films leading to graded structures. SAW experiments have shown that depending on the processing conditions, the porosity may be open or closed (restricted). The open porosity is monosized. Upon pyrolysis, lamellar structures collapse, while the hexagonal structures persist. When both hexagonal and lamellar structures are present, the hexagonal phase may serve to pillar the lamellar phase avoiding its complete collapse.

Figure 8 shows a scheme to create thick films that exploits the development and collapse of lamellar phases. As shown in **Step 1**, thick lamellar films can be prepared because the surfactant mechanically decouples stress development in adjoining layers. Upon drying and heating, each individual layer is free to shrink due to continuing condensation reactions without accumulation of stress. During surfactant pyrolysis the individually densified layers coalesce to form a thick crack-free layer. Initial experiments have shown feasibility of this idea.

With regard to closed porosity films, two ideas emerge. First it is likely that films prepared with low surfactant concentrations contain (randomly ordered) spherical micelles. Pyrolysis of the surfactant followed by sintering of the surrounding microporous silica matrix should lead to occlusion of spherical pores in a dense matrix. Second, by varying the initial surfactant concentration, we should be able to develop composite structures where, due to surfactant concentration at the film-vapor interface, a lamellar skin is formed over a hexagonal substructure. Pyrolysis then collapses the skin to form a barrier coating over the underlying mesoporous film. This idea may explain the SAW results shown in Figure 7 - where one film exhibits inaccessible porosity.

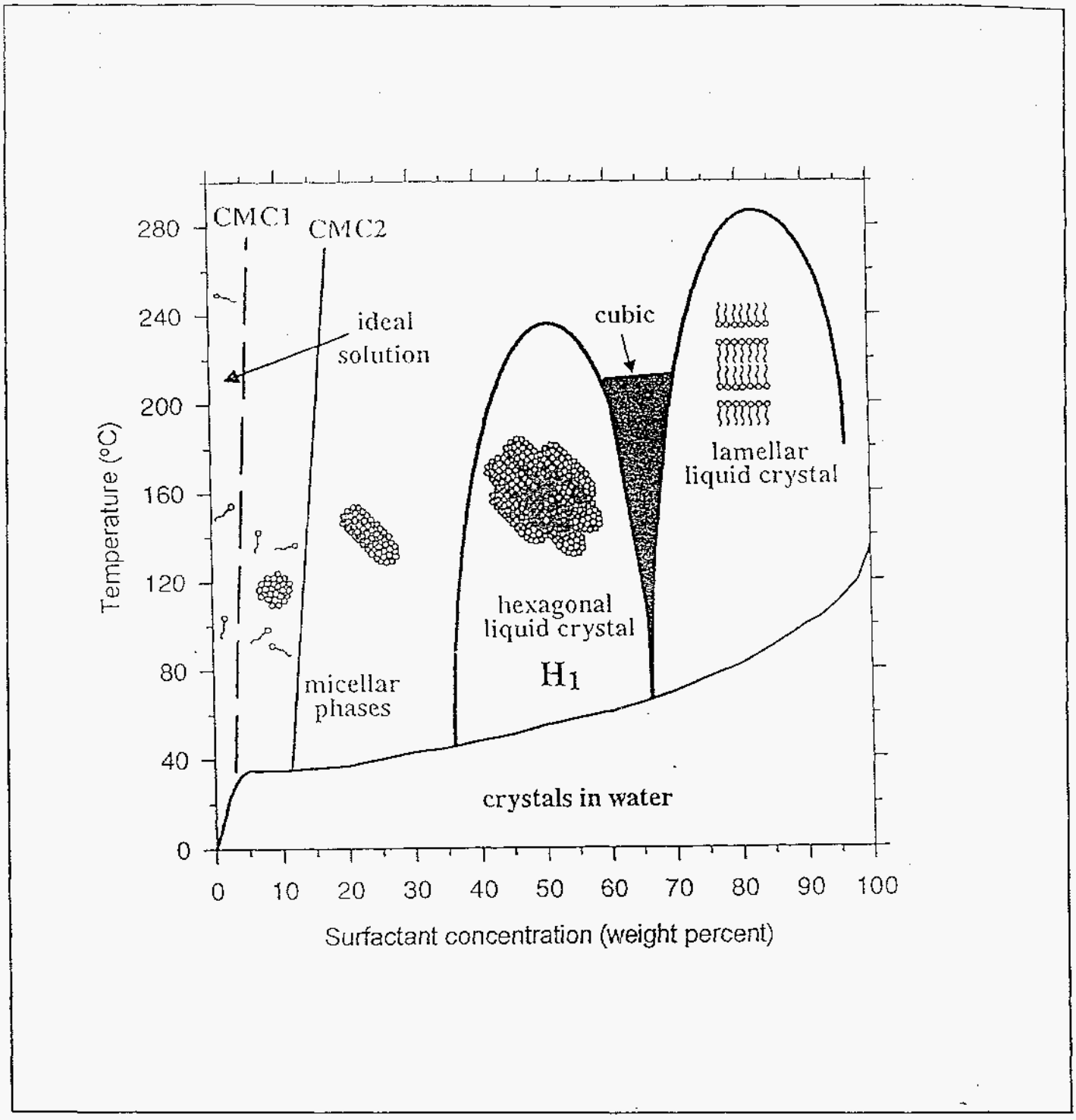

Fig 1. The evolution of macromolecular surfactant assemblies with increase in surfactant concentration (reproduced with permission from Anderson. M.).

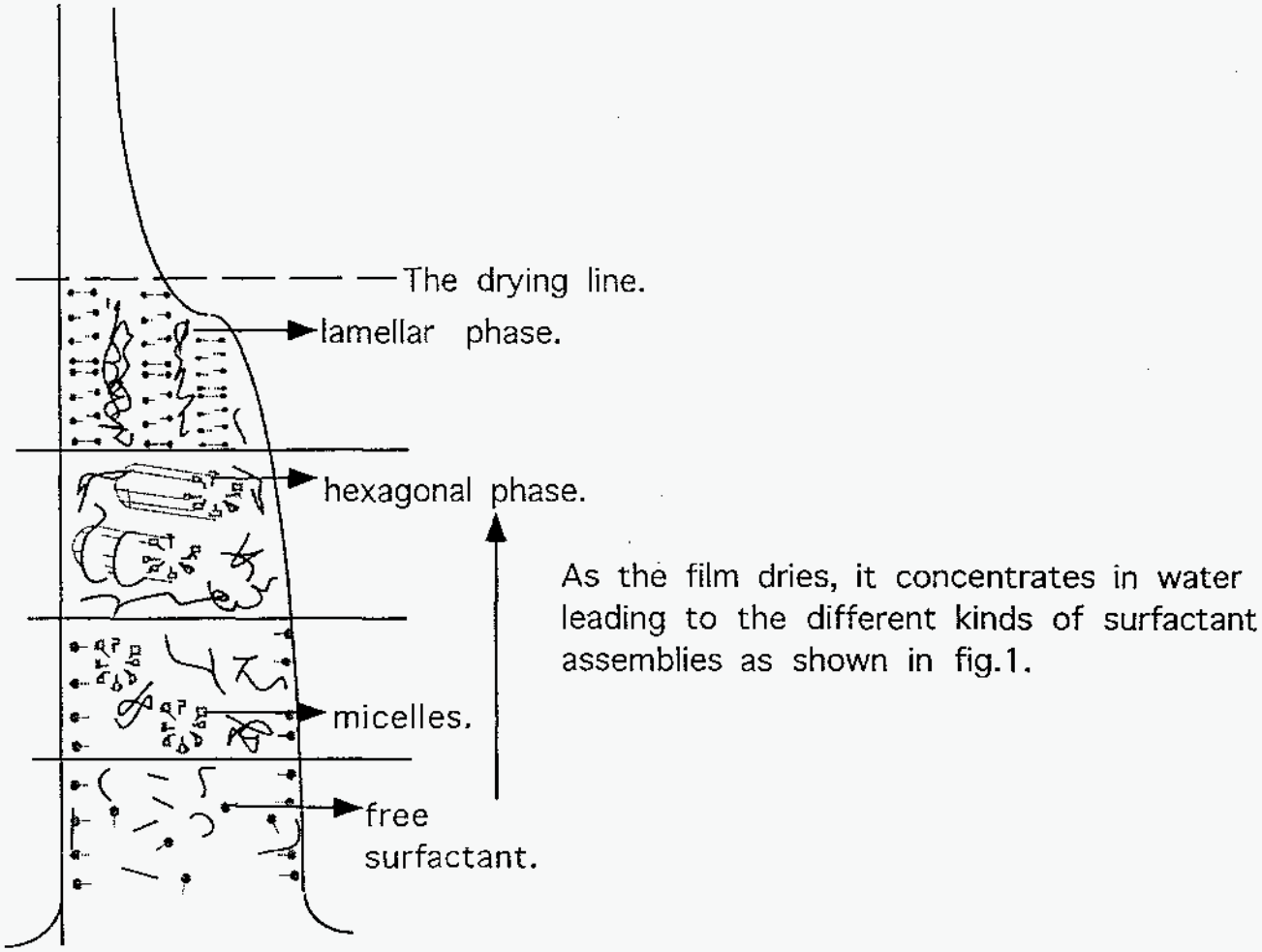

Fig 2. The gradual evolution of mesostructure in the dip coated film. The final mesostructure depends on the templating assembly at the drying line, where the final silica network locks in.

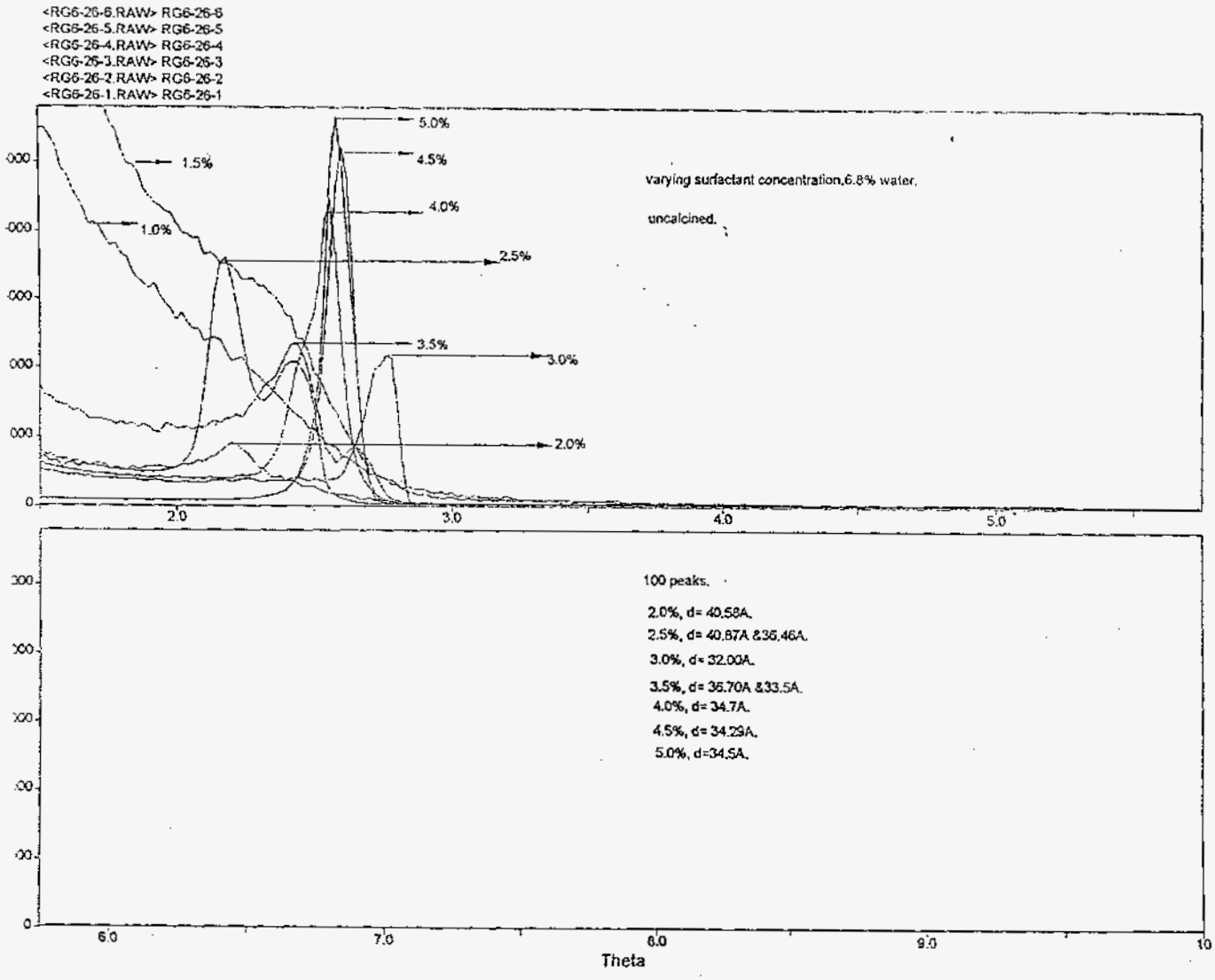

Laboratories AML

3(a). XRD results for uncalcined films with different surfactant concentrations.

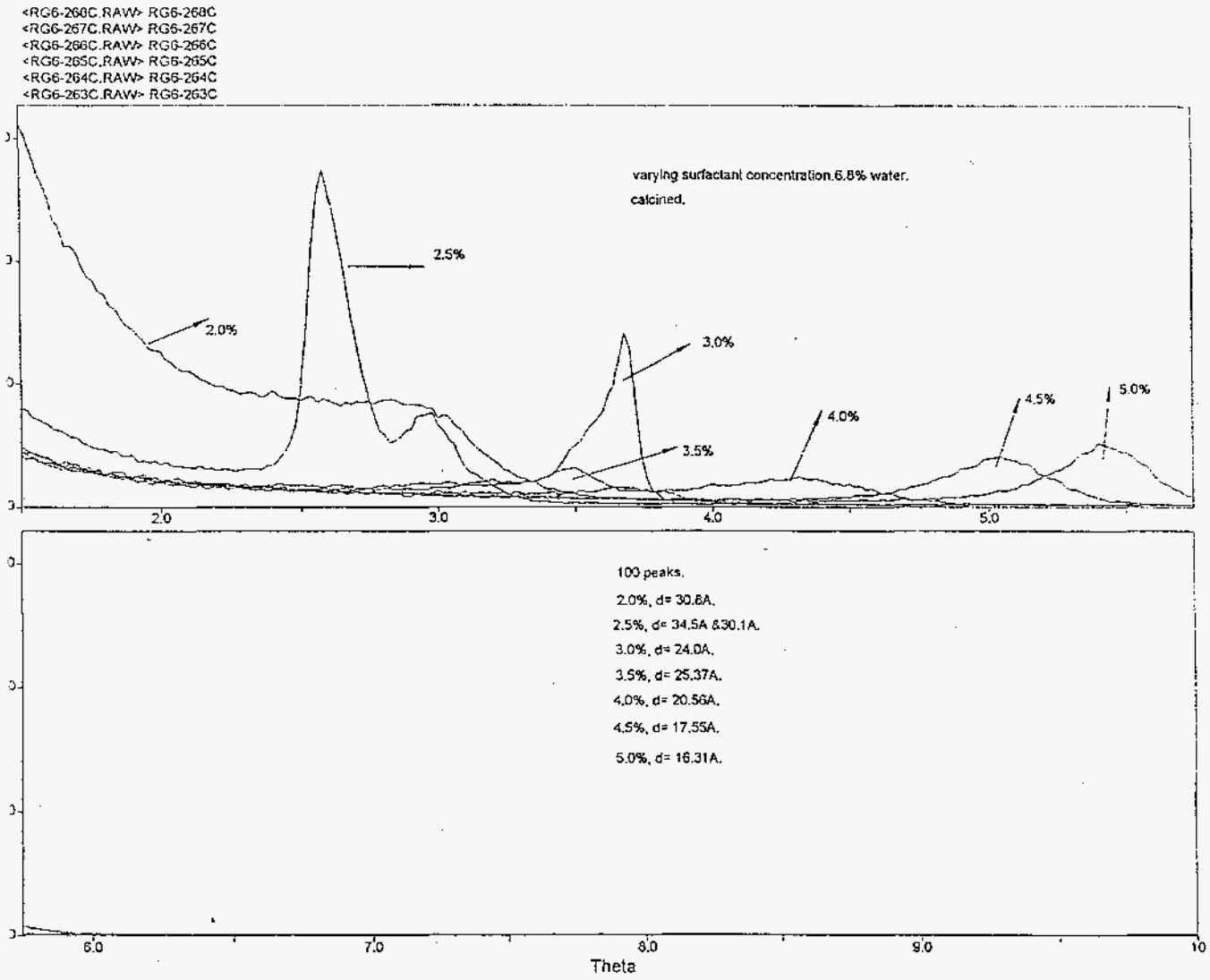

tboratories AML

c:\users\data\ganguli\ Saturday, Sep 14, 1996 @04:55p

3(b) XRD results for calcined films with different surfactant concentrations.

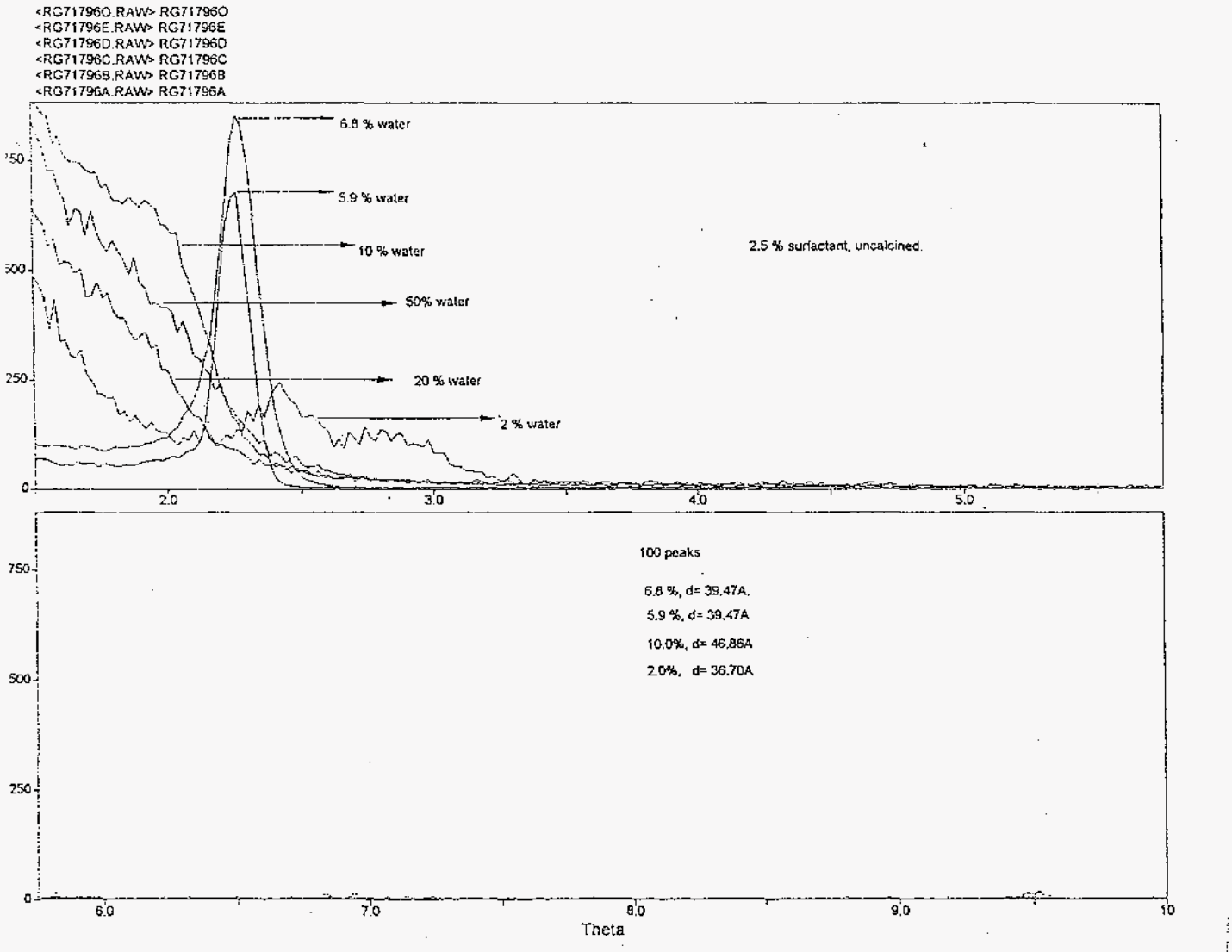

g 4(a) XRD results for uncalcined films with different water concentrations.

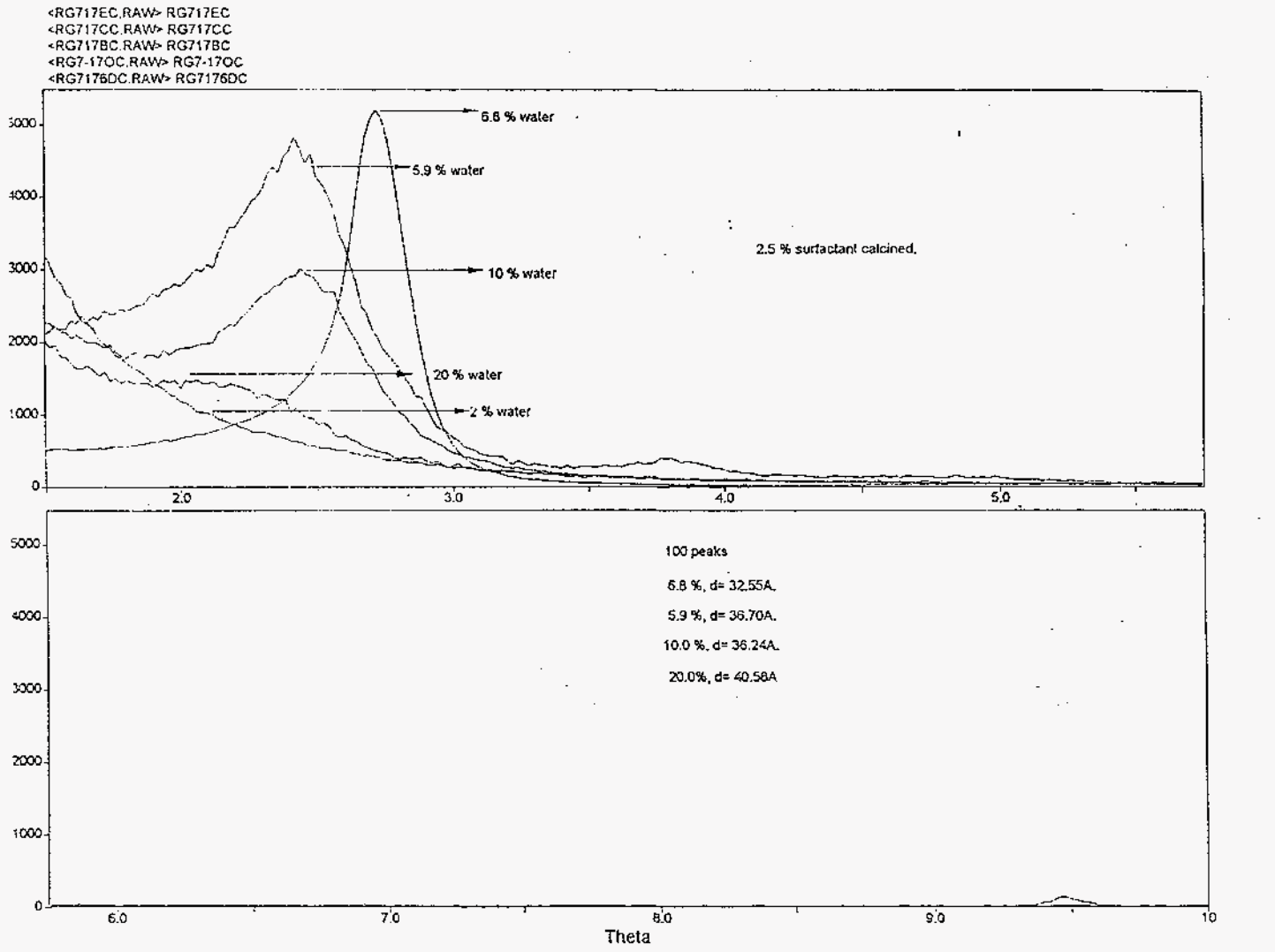

al Laboratories AML

<c:\userdata\gangulis> Saturday, Sep 14, 1996 @03:28p

lg 4(b) XRD results for calcined films with different water concentrations.

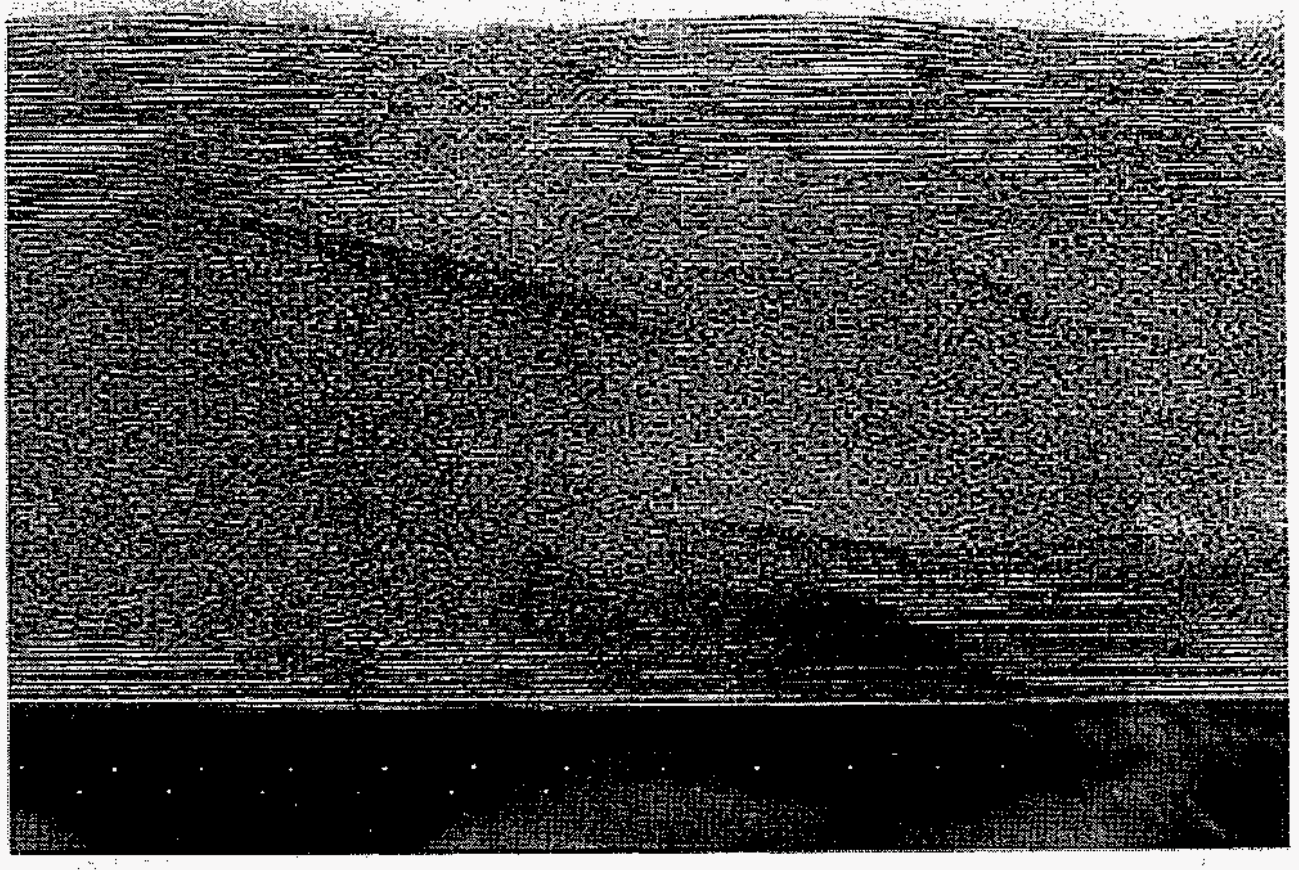

Fig 5. Cross sectional TEM for 6.8 % water and 2.5% surfactant film after calcination.

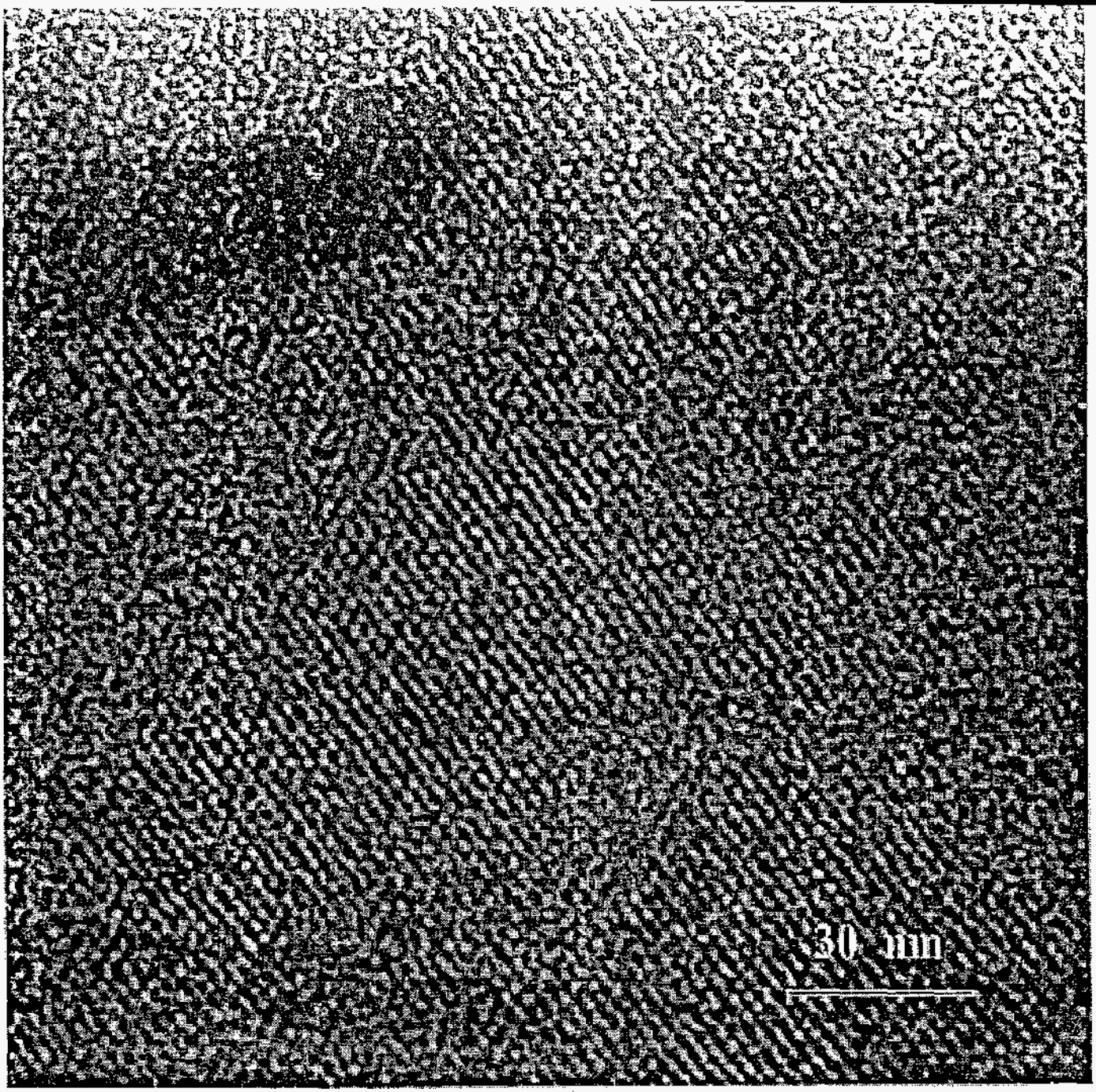

Fig 6. Plan view of calcined film with 5% surfactant dried at 90% relative humidity.

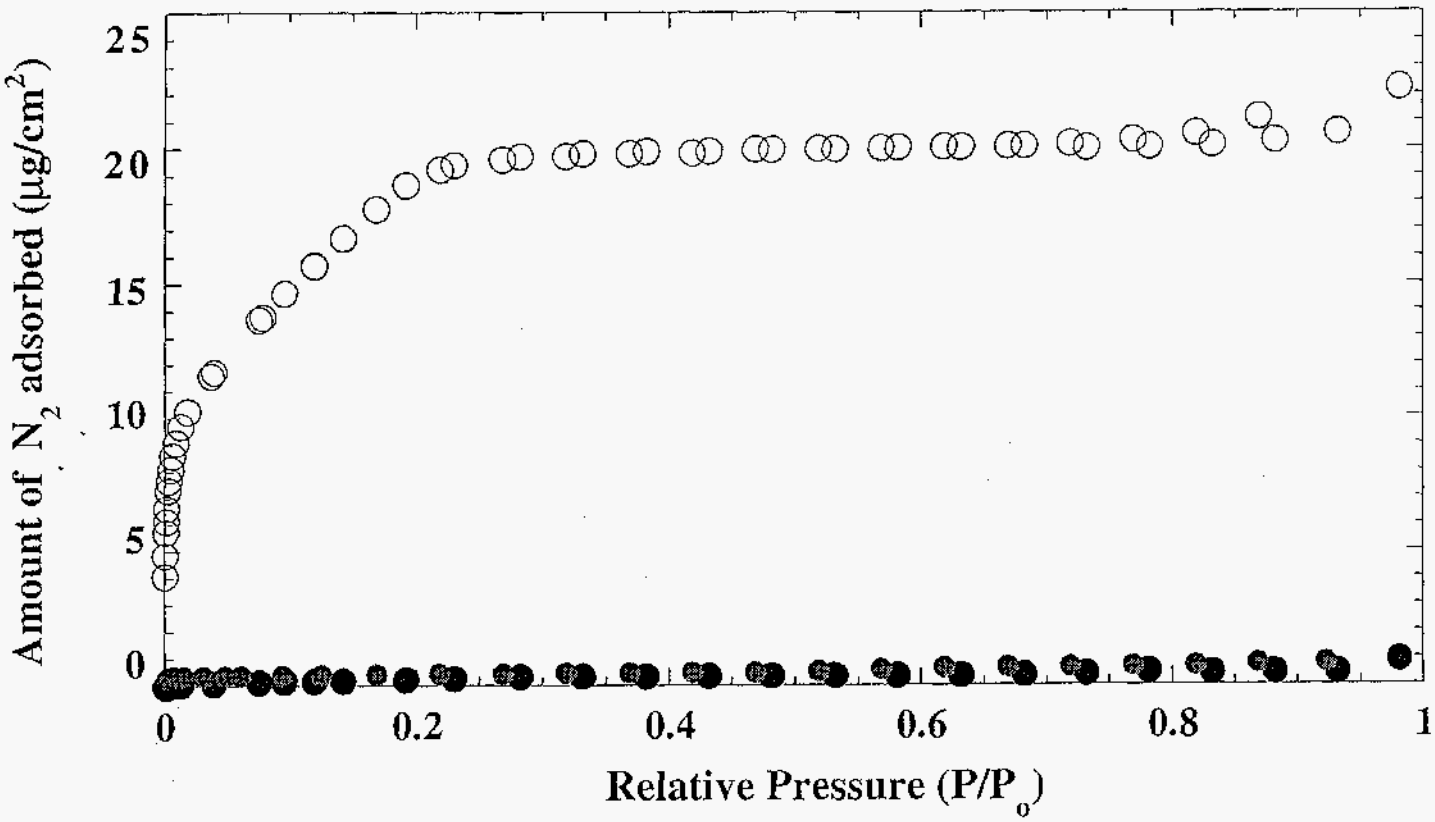

Fig 7 SAW adsorption isotherm of calcined films indicating both closed and open porosity.

Thickness of films in conventinal film preparation is limited by a critical cracking thickness, h_c

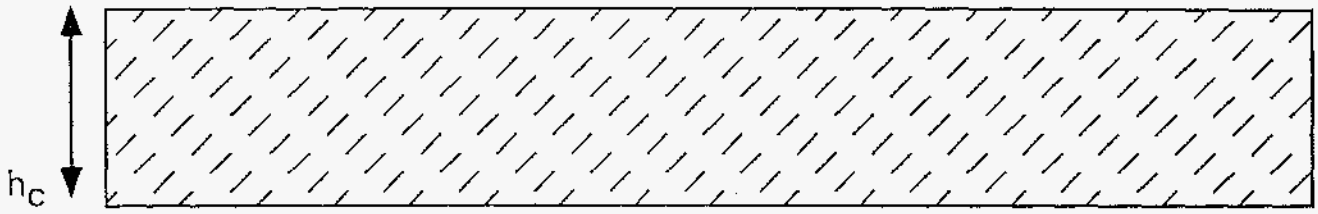

A way to get around this is to create silica-surfactant layers, and then when the film is pyrolyzed the surfactant leaves creating a thick silica film.

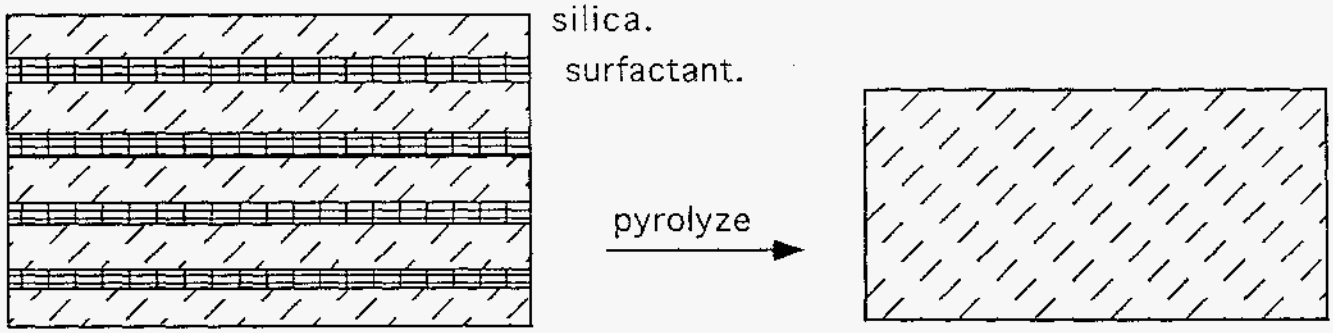

Step 1, Formation of silica-sufactant nanocomposite.

Step 2, Pyrolysis of nanocomposite to give thick silica film.

Fig 8 Possible mechanism of creating thick silica films.